The reaction $np \to \eta d$ near threshold

H. Garcilazo[1] and M. T. Peña[2,3]
[1]*Escuela Superior de Física y Matemáticas, Instituto Politécnico Nacional, Edificio 9, 07738 México D.F., Mexico*
[2]*Centro de Física das Interacções Fundamentais, Avenida Rovisco Pais, P-1049-001 Lisbon, Portugal*
[3] *Departamento de Física, Instituto Superior Técnico, Avenida Rovisco Pais, P-1049-001 Lisbon, Portugal*
(Received 2 April 2002; published 6 September 2002)

We have calculated the cross section for the process $np \to \eta d$ in the region near threshold, within the framework of a three-body model. We studied the dependence of the cross section to the production mechanism and to the initial- and final-state interactions. We found that the magnitude of the cross section is highly dependent on the reaction mechanism. However, its shape is essentially determined by the ηd final-state interaction alone. This strong signature in turn directly provides information about the ηN scattering length. For a variety of reaction mechanisms it is verified that the $np \to \eta d$ experimental data can only be explained if the ηN scattering length has a small real part, as it happens, for instance, in the ηN interaction model proposed recently by the Jülich group.

DOI: 10.1103/PhysRevC.66.034606 PACS number(s): 14.40.Aq, 25.40.Ve, 25.80.Hp

I. INTRODUCTION

The reaction $np \to \eta d$ has been measured recently in the region near threshold [1,2]. Since the cross section shows a strong enhancement at threshold, as compared with the predictions based on a two-body phase space, it has been speculated that this could be a signal for an ηNN quasibound state, predicted some time ago [3]. However, as we have pointed out recently [4,5] the solutions of the Faddeev equations for ηd elastic scattering do not support the existence of a ηNN quasibound state. Nevertheless, the strong ηN interaction in the resonant S_{11} channel is indeed responsible for an enhancement of the elastic scattering amplitude near threshold. Accordingly, it is logical to assume that in the reaction $np \to \eta d$ near threshold the ηd final-state interaction will produce a similar enhancement. In this work we investigate such a threshold effect by testing, in a three-body calculation for the ηNN system, different ηN dynamical models based upon recent data analysis of the coupled reactions $\pi N \to \eta N$, $\eta N \to \eta N$, and $\gamma N \to \eta N$. The $\eta d \to \eta d$ three-body transition matrix, describing the multiple scattering series for the ηd final-state interaction, is obtained by solving the Faddeev equations for the ηNN system (for such types of calculations see also, e.g., Refs. [6,7]). In addition, the present calculation provides some information on the large uncertainty region for the ηN scattering length, $a_{\eta N}$. The width of this region is defined by the considerable dispersion of empirical values originated by different data analysis.

In 1985 Bhalerao and Liu [8] constructed a coupled-channel model for threshold pionic eta production on a nucleon, which provided for the real part of $a_{\eta N}$ the value $\mathrm{Re}(a_{\eta N}) = 0.27$ fm. Later, Bennhold and Tanabe [9], in a study of η photoproduction reactions from nuclei, found a similar value, $\mathrm{Re}(a_{\eta N}) = 0.25$ fm. Also, a calculation of η and K photoproduction by Kaiser *et al.* [10] gave $\mathrm{Re}(a_{\eta N}) = 0.20$ fm. Other analyses [11–14], based on $\pi N - \pi N$, $\pi N - \eta N$, and $\gamma N - \eta N$ amplitudes, generated values within the higher value $0.72 - 1.07$ fm region. In 1993, Wilkin [15] reproduced the particular energy dependence of the cross section for $pd \to \eta^3\mathrm{He}$ with the value $\mathrm{Re}(a_{\eta N}) = 0.55$ fm. More recently [16] a model from the Julich group ascribes $\mathrm{Re}(a_{\eta N}) = 0.42$ fm.

II. FORMALISM

A. Two-body interactions

We will consider a nonrelativistic three-body model of the ηNN system, where the elementary ηN interaction will be obtained from a separable potential model of the coupled ηN-πN-σN system. Here, σN represents effectively the $\pi\pi N$ channel, which is a decay mode of the S_{11} resonance, corresponding to a 10% branching ratio. Therefore, we will take $m_\sigma = 2m_\pi$. Thus, we have replaced the three-body $\pi\pi N$ state by an effective two-body σN state. A more realistic description of the $\pi\pi N$ channel could be obtained by using for the σ the $I = J = 0\, \pi\pi$ resonance with an energy-dependent width determined by the $\pi\pi$ S-wave phase shift [17]. However, since the $\pi\pi N$ channel represents only about 10% of the width of the S_{11} resonance such a more sophisticated treatment may not be required.

In Refs. [4,5] we constructed and used six different phenomenological models of the coupled ηN-πN system, which were fitted only to the $\eta N \to \eta N$ amplitudes of recent data analyses [11–14]. In the present work we modified and extended these models by

(i) including a third channel (the σN channel) which represents the $\pi\pi N$ inelasticity,

(ii) fitting not only the $\eta N \to \eta N$ amplitude but also the $\pi^- p \to \eta n$ cross section, which is a direct source of information on the nondiagonal transition amplitude $\pi N \to \eta N$, and

(iii) considering the new amplitude analysis of the Jülich group [16] which leads to a ηN scattering length with a much smaller real part.

The six models based on the analyses [11–14] are labeled 1–6. They are updated versions in the sense of points (i) and (ii) above, of the corresponding models 1–6, introduced in

TABLE I. Parameters of the ηN-πN separable potential models fitted to the S_{11} resonant amplitudes given in Refs. [16,11–14].

Model	Reference	$a_{\eta N}$	α_η	A_η	λ_η	α_π	A_π	λ_π	α_σ	λ_σ
0	[10]	$0.42+i0.34$	5.8	4.274 065	−402.494 242	0.85	0.084 033	−0.103 387	4.0	−31.393 844
1	[7]	$0.72+i0.26$	11.51	13.721 902	−3409.633 910	2.5	0.333 333	−0.233 452	8.0	−337.208 962
2	[8]	$0.75+i0.27$	34.0	727.456 846	−9680.979 572	7.65	0.125	−303.773 097	8.0	−949.290 930
3	[9](D)	$0.83+i0.27$	37.0	1375.158 782	−5714.431 017	7.9	0.126 582	−355.276 424	8.0	−768.503 721
4	[9](A)	$0.87+i0.27$	29.0	725.390 756	−2970.266 050	8.05	0.124 223	−397.637 234	8.0	−613.614 034
5	[9](B)	$1.05+i0.27$	6.0	31.656 004	−4.875 780	9.0	0.104 602	−686.689 630	8.0	−187.838 543
6	[9](C)	$1.07+i0.26$	5.5	209.617 836	−0.044 430	9.6	0.113 636	−823.579 746	8.0	−159.526 035

Ref. [4]. The model based on the Jülich data analysis is newly considered here and is labeled by "0."

The potentials describing the meson-nucleon transitions in all the models built here are of separable form,

$$\langle p|V_{ii}|p'\rangle=\lambda_i g_i(p)g_i(p') \quad (i=\eta,\pi,\sigma), \tag{1}$$

$$\langle p|V_{ij}|p'\rangle=\pm\sqrt{\lambda_i\lambda_j}g_i(p)g_j(p') \quad (i,j=\eta,\pi,\sigma) \tag{2}$$

with

$$g_\eta(p)=\frac{A_\eta+p^2}{(\alpha_\eta^2+p^2)^2}, \tag{3}$$

$$g_\pi(p)=\frac{A_\pi+p^2}{(\alpha_\pi^2+p^2)^2}, \tag{4}$$

$$g_\sigma(p)=\frac{p}{(\alpha_\sigma^2+p^2)^2}, \tag{5}$$

where the ηN and πN form factors correspond to S waves, while the σN form factor corresponds to a P wave, as required by parity conservation.

The Lippmann-Schwinger coupled-channel equations for the meson-nucleon system generate from the potentials (1) and (2) the meson-nucleon t matrices are

$$\langle p|t_{\eta\eta}(E)|p'\rangle=g_\eta(p)\tau_2(E)g_\eta(p'), \tag{6}$$

$$\langle p|t_{\pi\pi}(E)|p'\rangle=\frac{\lambda_\pi}{\lambda_\eta}g_\pi(p)\tau_2(E)g_\pi(p'), \tag{7}$$

$$\langle p|t_{\eta\pi}(E)|p'\rangle=\pm\sqrt{\frac{\lambda_\pi}{\lambda_\eta}}g_\eta(p)\tau_2(E)g_\pi(p'), \tag{8}$$

$$\langle p|t_{\eta\sigma}(E)|p'\rangle=\pm\sqrt{\frac{\lambda_\sigma}{\lambda_\eta}}g_\eta(p)\tau_2(E)g_\sigma(p'), \tag{9}$$

where $\tau_2(E)$ gives the dressed S_{11} resonance propagator, its inverse corresponding to a sum of a Dyson series, for the ηN, πN, and σN channels,

$$\frac{1}{\tau_2(E)}=\frac{1}{\lambda_\eta}-G_\eta(E)-\frac{\lambda_\pi}{\lambda_\eta}G_\pi(E)-\frac{\lambda_\sigma}{\lambda_\eta}G_\sigma(E), \tag{10}$$

with E the ηN c.m. kinetic energy, and

$$G_\eta(E)=\int_0^\infty p^2dp\,\frac{g_\eta^2(p)}{E-p^2/2\mu_\eta+i\epsilon}, \tag{11}$$

$$G_\pi(E)=\int_0^\infty p^2dp\,\frac{g_\pi^2(p)}{E+m_N+m_\eta-\sqrt{m_N^2+p^2}-\sqrt{m_\pi^2+p^2}+i\epsilon}, \tag{12}$$

$$G_\sigma(E)=\int_0^\infty p^2dp\,\frac{g_\sigma^2(p)}{E+m_N+m_\eta-\sqrt{m_N^2+p^2}-\sqrt{m_\sigma^2+p^2}+i\epsilon}. \tag{13}$$

In the equations above we have used relativistic kinematics for the πN and σN channels.

The parameters of the ηN, πN, and σN form factors given by Eqs. (3)–(5) are given in Table I. In Fig. 1 we show the comparison between our models and the amplitudes of Refs. [16,11–14] as well as the prediction of our models for the $\pi^- p\to\eta n$ cross section. We note that the fitting procedure in Ref. [4] used only the data analysis of the $\eta N\to\eta N$ transition. Thus, only Eq. (6) was used for the fit, while the g_π coupling appearing in Eqs. (7) and (8) was only indirectly fixed through its presence in τ_2 [Eqs. (10)–(12)]. In contrast, in this work Eq. (8) is additionally used to constrain g_π and g_η by the $\pi^- p\to\eta n$ total cross-section data. In Sec. III A, the results obtained show a relatively small importance of the σN channel. Nevertheless, further studies may be needed in this respect, involving a nonzero width of the σ.

The separable potential for the NN subsystem in the $^3S_1$ channel is the so-called PEST model [18],

$$\langle p|V_{NN}|p'\rangle=-g_N(p)g_N(p'), \tag{14}$$

so that the nucleon-nucleon t matrix is

$$\langle p|t_{NN}(E)|p'\rangle=-g_N(p)\tau_1(E)g_N(p'), \tag{15}$$

with

$$\frac{1}{\tau_1(E)}=-1-\int_0^\infty p^2dp\,\frac{g_N^2(p)}{E-p^2/m_N+i\epsilon}. \tag{16}$$

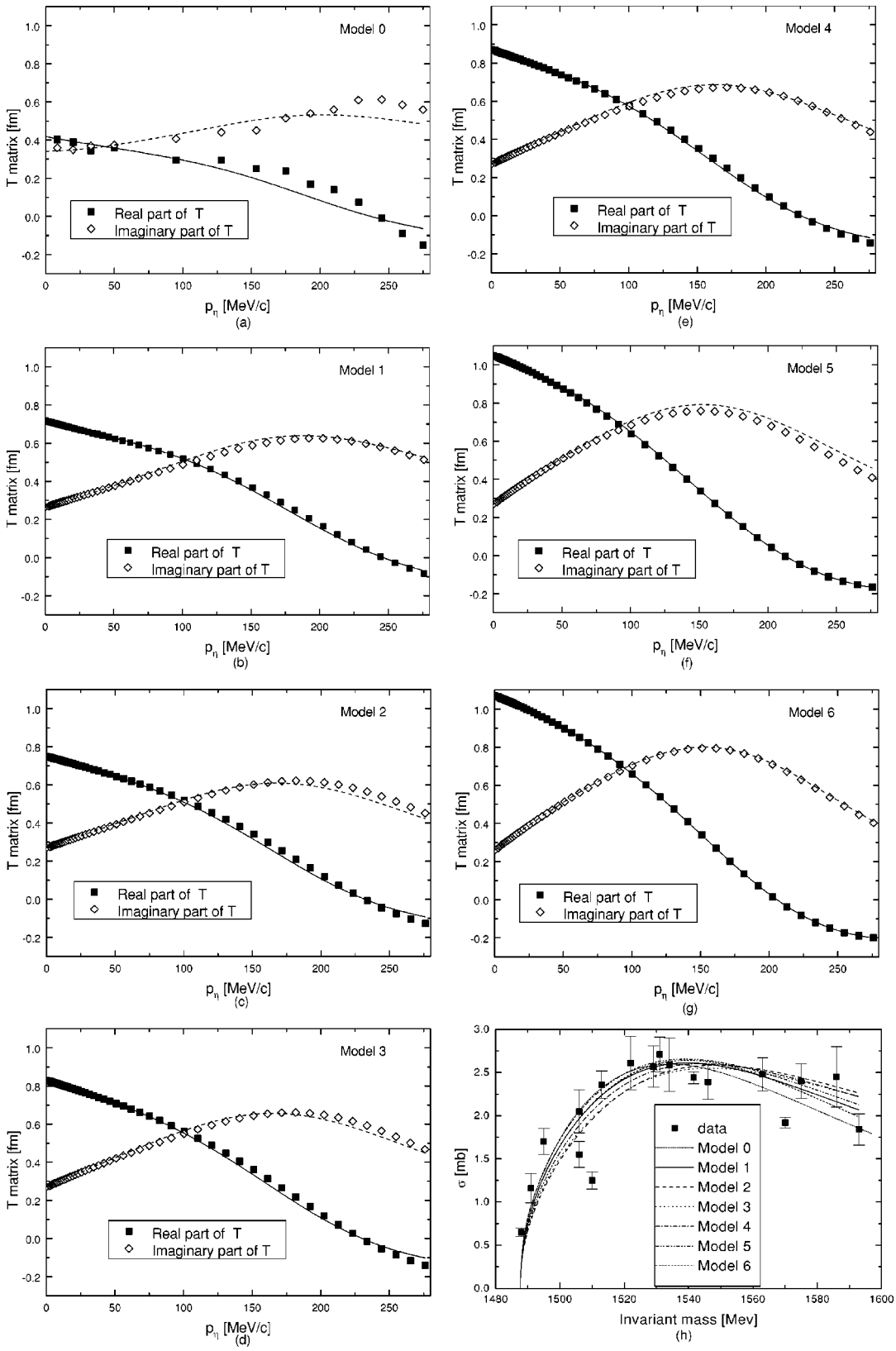

FIG. 1. Comparison of the $\eta N \to \eta N$ amplitudes produced by the separable potentials of Table I with the amplitude analysis of Refs. [16,11–14]. Also shown are the predictions of the models for the $\pi^- p \to \eta n$ cross section, where the experimental data have been compiled in Ref. [11].

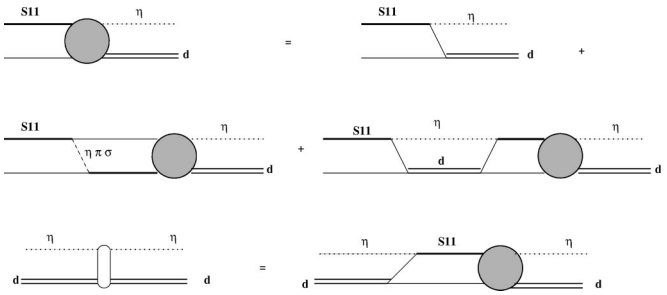

FIG. 2. Faddeev equations for ηd elastic scattering.

The form factor of the PEST interaction is given by

$$g_N(p)=\sum_{n=1}^{6}\frac{c_n}{\beta_n^2+p^2}, \tag{17}$$

with the parameters given in Ref. [18]. This model yields the same deuteron wave function as the Paris potential.

B. Faddeev equations for ηd scattering

We consider the system of three particles (η, N, and N), where two of them are identical, and all three interact through pairwise interactions. We represent these interactions with separable potentials. As for the possible three-body channels, we restrict the orbital states between spectator particles and the center of mass of interacting pairs to S waves ($\lambda=0$). In particular, for the channels with an η being a spectator, this truncation is a good approximation for energies near threshold, where the effect of the centrifugal barrier has to be small. As for the relative orbital momentum of the states for the different pairs, we also restrict these states to S waves, with the exception of the σ-N pair case: due to the intrinsic parity of the σ (two pions), the contribution to the S wave of the $\eta N\rightarrow\eta N$ amplitude yielded by a σ-N intermediate state comes necessarily from a P wave. For the ηd system, the relative orbital S-wave states for the interacting pairs are the S_{11} channel for the eta-nucleon pair, and the $^3S_1$ channel for the nucleon-nucleon pair.

We will identify particle 1 with the η and the identical particles 2 and 3 with the two nucleons. The Faddeev equations for ηd elastic scattering are shown diagrammatically in Fig. 2. In the second equation of this figure, there is a term with the nucleon-nucleon interaction proceeding while a meson is a spectator. That meson can only be the η. Indeed, the term with a pion as the spectator meson would imply an intermediate state (formed by a pion and an NN state in the $^3S_1$ channel) of isospin 1, whereas the ηd final system has isospin 0. Moreover, the intermediate state where a pion is the spectator and the NN state is in the $^1S_0$ scattering state cannot proceed either, due to the fact that this state has total spin 0, while the ηd system has total spin 1. As for the σ meson, it also does not contribute as a spectator to the scattering series due to conservation of parity, since we are restricting the orbital angular momentum between the spectator and the pair to be an S wave, and the final system has a total negative parity.

The integral equations of Fig. 2 are written analytically as

$$\begin{aligned}T_2(q_2;E)=&K_{21}(q_2,q_{10};E)+\int_0^\infty q_2'^2dq_2'K_{23}(q_2,q_2';E)\\&\times\tau_2(E-q_2'^2/2\nu_2)T_2(q_2';E)\\&+\int_0^\infty q_1^2dq_1K_{21}(q_2,q_1;E)\\&\times\tau_1(E-q_1^2/2\nu_1)T_1(q_1;E),\end{aligned} \tag{18}$$

$$\begin{aligned}T_1(q_1;E)=&2\int_0^\infty q_2^2dq_2K_{12}(q_1,q_2;E)\\&\times\tau_2(E-q_2^2/2\nu_2)T_2(q_2;E).\end{aligned} \tag{19}$$

The function $T_2(q_2;E)$ represents the transition amplitude from the ηd state to a state with a nucleon and a S_{11} isobar while the function $T_1(q_1;E)$ represents the transition amplitude from the ηd state to the ηd state.

The kernels of the integral Eqs. (18) and (19) are given by

$$K_{12}(q_1,q_2;E)=\frac{1}{2}\int_{-1}^{1}d\cos\theta\frac{g_N(p_1)g_\eta(p_2)}{E-p_1^2/2\mu_1-q_1^2/2\nu_1+i\epsilon}, \tag{20}$$

$$K_{21}(q_2,q_1;E)=\frac{1}{2}\int_{-1}^{1}d\cos\theta\frac{g_\eta(p_2)g_N(p_1)}{E-p_2^2/2\mu_2-q_2^2/2\nu_2+i\epsilon}, \tag{21}$$

$$\begin{aligned}K_{23}(q_2,q_3;E)=&\frac{1}{2}\int_{-1}^{1}d\cos\theta\frac{g_\eta(p_2)g_\eta(p_3)}{E-p_2^2/2\mu_2-q_2^2/2\nu_2+i\epsilon}-\frac{1}{2}\int_{-1}^{1}d\cos\theta\frac{g_\pi(p_{2\pi})g_\pi(p_{3\pi})}{E+m_\eta-m_\pi-p_{2\pi}^2/2\mu_\pi-q_2^2/2\nu_\pi+i\epsilon}\\&+\frac{1}{2}\int_{-1}^{1}d\cos\theta\frac{g_\sigma(p_{2\sigma})g_\sigma(p_{3\sigma})}{E+m_\eta-m_\sigma-p_{2\sigma}^2/2\mu_\sigma-q_2^2/2\nu_\sigma+i\epsilon}\frac{\cos\theta_{23}}{3}.\end{aligned} \tag{22}$$

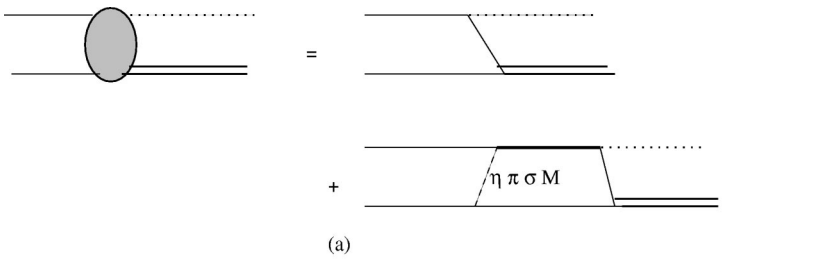

(a)

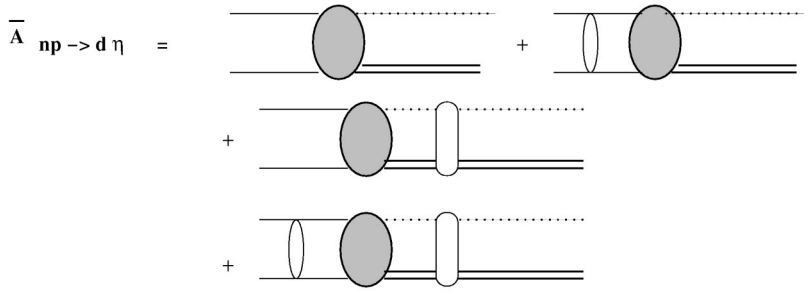

(b)

FIG. 3. Model of the $np \to \eta d$ process. (a) Direct-production diagram and box diagram including η, π, σ, and heavy meson exchanges. (b) *NN* initial-state interaction and ηd final-state-interaction diagrams.

μ_i and ν_i are the reduced masses

$$\mu_i = \frac{m_j m_k}{m_j + m_k}, \tag{23}$$

$$\nu_i = \frac{m_i (m_j + m_k)}{m_i + m_j + m_k}, \tag{24}$$

and the relative momenta p_i and p_j are

$$p_i = \left(\frac{\mu_i^2}{m_k^2} q_i^2 + q_j^2 + 2 \frac{\mu_i}{m_k} q_i q_j \cos\theta \right)^{1/2}, \tag{25}$$

$$p_j = \left(\frac{\mu_j^2}{m_k^2} q_j^2 + q_i^2 + 2 \frac{\mu_j}{m_k} q_i q_j \cos\theta \right)^{1/2}. \tag{26}$$

The corresponding relative momenta and reduced masses with subindex π or σ are obtained from Eqs. (23)–(26) by taking for m_1 the mass of the π or σ meson, respectively. Finally, $\cos\theta_{23}$ is given by

$$\cos\theta_{23} = \frac{m_\sigma}{2 \mu_{3\sigma} p_{3\sigma} p_{2\sigma}} \left[\left(\frac{\mu_{3\sigma} q_2}{\nu_{2\sigma}} \right)^2 - p_{3\sigma}^2 - \left(\frac{\mu_{3\sigma} p_{2\sigma}}{m_\sigma} \right)^2 \right]. \tag{27}$$

Even though for the two-body subsystems the π and the σ are treated relativistically, in the case of the three-body equations all particles are treated nonrelativistically.

Notice that in Eq. (22) the contribution of the η comes with a plus sign while the contribution of the π comes with a minus sign. These signs come from the reduction of the Faddeev equations when one has two identical fermions [19,20]. Since we are assuming that the meson is particle 1 so that 2 and 3 are the two fermions and for the π and η all orbital angular momenta are equal to zero, then following the reduction procedure of Refs. [19,20] leads to the result that the kernel K_{23} must by multiplied by a factor F_{23}, where

$$F_{23} = F_{23}^{Iden} F_{23}^{spin} F_{23}^{isospin}, \tag{28}$$

and

$$F_{23}^{iden} = -(-)^{s_1 + s_3 - S_2 + i_1 + i_3 - I_2}, \tag{29}$$

$$F_{23}^{spin} = (-)^{S_3 + s_3 - S} \sqrt{(2S_2+1)(2S_3+1)}\, W(s_3 s_1 S s_2; S_2 S_3), \tag{30}$$

$$F_{23}^{isospin} = (-)^{I_3 + i_3 - I} \sqrt{(2I_2+1)(2I_3+1)}\, W(i_3 i_1 I i_2; I_2 I_3), \tag{31}$$

with W the Racah coefficient, and s_i, S_i, and S (i_i, I_i, and I) are the spins (isospins) of particle i, the pair jk, and the three-body system. It is straightforward to see that the factor F_{23} is equal to 1 when particle 1 is a η but it is equal to -1 when particle 1 is a π. In the case of the σ the orbital angular momentum of the pair and the total orbital angular momentum are $l = L = 1$ so that the derivation of the kernel is slightly more complicated as shown, for example, in Ref. [20] with the result that appears in the last term of Eq. (22).

C. The production mechanism

In Fig. 3 we represent the model considered in this work for the mechanism of the $np \to \eta d$ reaction. Figure 3(a) shows the driving terms for the meson production reaction, which consist of the direct-production diagram and of the box diagram, containing the rescattering of the η, π, and σ mesons plus other heavy meson exchanges (generically la-

beled by M) through excitation of the S_{11} resonance. Figure 3(b) shows the distortion of the driving terms by the initial- and final-state interactions.

The initial-state interaction is calculated using a two-body NN distorted wave function

$$\Psi q_{N0}(q_N)=\frac{1}{q_N^2}\delta(q_N-q_{N0})+\frac{m_N}{q_{N0}^2-q_N^2+i\epsilon}T_{NN}(q_N;E), \tag{32}$$

where q_{N0} is the NN on-shell momentum given by

$$q_{N0}^2=\frac{(2m_N+m_\eta+E)^2}{4}-m_N^2, \tag{33}$$

$m_N/(q_{N0}^2-q_N^2+i\epsilon)$ is the Lippmann-Schwinger propagator of the NN system, and $T_{NN}(q_N;E)$ is the half-shell nucleon-nucleon t matrix which will be discussed in the next subsection.

As for the final-state interaction, it is treated using a three-body distorted wave involving $\tau_1(E-q_1^2/2\nu_1)$, the propagator of an NN isobar and a spectator η defined by Eq. (16), and $T_1(q_1;E)$, the $\eta d\to\eta d$ three-body scattering amplitude obtained from the solution of the integral Eqs. (18) and (19).

The effect of the initial- and final-state interactions is thus given by the two-loop calculation

$$\begin{aligned}\overline{A}_{np\to\eta d}=&\int_0^\infty q_1^2dq_1\int_0^\infty q_N^2dq_N\left[\frac{1}{q_1^2}\delta(q_1-q_{10})\right.\\&\left.+\tau_1(E-q_1^2/2\nu_1)T_1(q_1;E)\right]A_{np\to\eta d}(q_1,q_N)\\&\times\left[\frac{1}{q_N^2}\delta(q_N-q_{N0})+\frac{m_N}{q_{N0}^2-q_N^2+i\epsilon}T_{NN}(q_N;E)\right].\end{aligned} \tag{34}$$

The production amplitude without initial- and final-state interactions $A_{np\to\eta d}(q_1,q_N)$ which appears in Eq. (34) is shown diagrammatically in Fig. 3(a). In order to make the Feynmann diagrams in this figure consistent with the Faddeev diagrams of Fig. 2 their nonrelativistic limit is taken and their projections on the initial $NN\ {}^1P_1$ channel and final $\eta d\ {}^3S_1$ channel are performed.

If we start with pseudovector coupling for the π and the η the ηNN vertex in the nonrelativistic limit becomes the Galilean-invariant form

$$\begin{aligned}V_{\eta NN}=&\frac{f_\eta}{m_\eta}\vec{\sigma}\cdot\left[\vec{k}_\eta-\frac{m_\eta}{2m_N}(\vec{k}_N+\vec{k}_N')\right]\\\approx&\frac{f_\eta}{m_\eta}\vec{\sigma}\cdot\left[\vec{k}_\eta-\frac{m_\eta}{m_N}\vec{k}_N\right]\\=&\frac{f_\eta}{m_\eta}\left(1+\frac{m_\eta}{m_N}\right)\vec{\sigma}\cdot\frac{m_N\vec{k}_\eta-m_\eta\vec{k}_N}{m_N+m_\eta}\\=&\frac{f_\eta}{m_\eta}\left(1+\frac{m_\eta}{m_N}\right)\vec{\sigma}\cdot\vec{p},\end{aligned} \tag{35}$$

where $\vec{p}$ is the relative momentum between the meson and the nucleon and the approximation that we have made, $\vec{k}_N'=\vec{k}_N+\vec{k}_\eta\approx\vec{k}_N$, is exact for the direct term at threshold where $\vec{k}_\eta=0$. Similarly, the πNN and σNN vertices are

$$V_{\pi NN}=\frac{f_\pi}{m_\pi}\left(1+\frac{m_\pi}{m_N}\right)\vec{\sigma}\cdot\vec{p}\,\vec{\tau}\cdot\vec{\phi}_\pi, \tag{36}$$

$$V_{\sigma NN}=f_\sigma. \tag{37}$$

If instead we start with pseudoscalar coupling we would get

$$V_{\eta NN}=\frac{f_\eta}{m_\eta}\vec{\sigma}\cdot\vec{k}_\eta, \tag{38}$$

where $\vec{k}_\eta$ is the momentum of the η, and similarly for the pion. We will introduce a form factor that regularizes the vertices at large momenta as

$$V_{mNN}\to V_{mNN}\frac{\Lambda^2+p_0^2}{\Lambda^2+p^2}, \tag{39}$$

where p_0 is the on-shell momentum. We took for the cutoff parameter $\Lambda=1800$ MeV/c which is a typical value for meson-exchange models [21,22]. The on-shell momentum p_0 is given by

$$p_0^2=\frac{[s-(M-\mu)^2][s-(M+\mu)^2]}{4s}, \tag{40}$$

where M and μ are the nucleon and meson masses, respectively, and

$$s=M^2. \tag{41}$$

The meson-nucleon couplings with the S_{11} isobar are specified by the separable potential models of the coupled ηN-πN-σN system described above. We also included in the driving terms the contribution of the heavy mesons η' and σ' with masses of 958 and 980 MeV, and nucleon vertex functions similar to Eqs. (35) and (37), respectively. We note that the coupling vertex of one of these mesons with the S_{11} is the coupling vertex of the other one with the nucleon, due to parity. We took the πNN coupling constant value $f_\pi=0.079$, and $m_\sigma=2m_\pi$ and $f_\sigma=0.798$, as given in Ref. [23].

D. The NN initial-state interaction

The initial-state nucleon-nucleon interaction for this problem is needed at energies well above the pion-production threshold, and no realistic NN potential built so far is valid

for this energy range, and describes satisfactorily the nonvanishing nucleonic inelasticities. Therefore,we constructed a purely phenomenological extension of the Paris NN potential, to those energies, by including an energy dependent adjustable imaginary term

$$V(p,p') = V_{Paris}(p,p') - i\gamma \frac{pp'}{(\alpha^2+p^2)(\alpha^2+p'^2)}. \tag{42}$$

The parameters $\gamma = 0.6$ and $\alpha = 0.75$ fm^{-1} were obtained by fitting the experimental amplitude of Arndt *et al.* [24] very near the η production energy threshold. The NN amplitude in the $^1P_1$ initial nucleonic channel could then be calculated from the Lippman-Schwinger equation with the complex potential above tuned this way. As a result, the NN initial-state interaction yields a suppression of the cross section of a factor 5 (i.e., the cross section gets multiplied by a factor 0.2), approximately a constant reduction factor, as usually assumed for the nucleon-nucleon interaction at high energies [25,26].

It is interesting to compare our tratment of the initial-state interaction with other methods proposed in the literature. Hanhart and Nakayama [27], for example, neglect the principal part in the last integration of Eq. (34), i.e., they assume

$$\frac{m_N}{q_{N0}^2 - q_N^2 + i\epsilon} \to -\pi i m_N \delta(q_{N0}^2 - q_N^2). \tag{43}$$

Fäldt and Wilkin [28], on the other hand, multiply the production amplitude by the factor $e^{-\mathrm{Im}(\delta_L)}$ so that the cross section gets multiplied by the factor $e^{-2\mathrm{Im}(\delta_L)}$. With our potential (42) we get at the η threshold a $^1P_1$ nucleon-nucleon amplitude (in Argand diagram normalization) of $(-0.244, 0.583)$. Using this amplitude, the Hanhart and Nakayama prescription gives a reduction factor of 0.233 which is 17% larger than our reduction factor of 0.2. The Fäldt and Wilkin prescription, on the other hand, gives a reduction factor of 0.515 which is more than twice the reduction factor obtained with either ours or Hanhart and Nakayama's prescriptions.

III. RESULTS

A. The ηd elastic channel

We started by calculating the ηd scattering length and elastic cross section in order to compare with our previous results [4,5].

We present in Table II the predictions for the ηd scattering length of the seven separable models for the coupled ηN-πN-σN system. We show the results obtained considering

(i) η exchange only in the Faddeev equations of Fig. 2 [only the first term in the right hand side of Eq. (22)],

(ii) η and π exchange [the first and second terms in the right hand side of Eq. (22)],

(iii) η-π and σ exchange [all three terms in the right hand side of Eq. (22)].

TABLE II. ηd scattering length (in fm) predicted by the seven separable potential models of the coupled ηN-πN-σN system. We give the results obtained including only η exchange, η and π exchange, and η-π and σ exchange in the driving terms of Fig. 2.

Model	$a_{\eta N}$	η	$\eta+\pi$	$\eta+\pi+\sigma$
0	$0.42+i0.34$	$1.01+i1.24$	$1.00+i1.28$	$0.99+i1.28$
1	$0.72+i0.26$	$2.53+i1.51$	$2.56+i1.51$	$2.57+i1.51$
2	$0.75+i0.27$	$2.75+i1.64$	$2.75+i1.62$	$2.76+i1.62$
3	$0.83+i0.27$	$3.28+i1.93$	$3.28+i1.91$	$3.30+i1.91$
4	$0.87+i0.27$	$3.55+i2.07$	$3.56+i2.05$	$3.57+i2.04$
5	$1.05+i0.27$	$4.91+i2.72$	$4.92+i2.70$	$4.93+i2.70$
6	$1.07+i0.26$	$4.77+i2.25$	$4.79+i2.25$	$4.79+i2.24$

Table II evidences that the η contribution is the dominant one, with the π and σ contributions having a very small effect on the ηd scattering length.

In the previous work of Ref. [5] the pion contribution was much larger, due to the fact that the $\eta N \to \pi N$ transition amplitude was not sufficiently well constrained by the separable potentials. Consequently, those first models lead to a $\pi^- p \to \eta n$ cross section two to three times larger than the experimental one shown in Fig. 1. Our new results exhibit a smaller effect from the pion rescattering contribution and are thus consistent with the results found by Fix and Arenhövel [29] and Wycech and Green [30].

In spite of the new feature just mentioned, the new results, as the previous ones [4,5], do not imply the existence of a ηNN quasibound state (whose signature is that the real part of the ηd scattering length becomes negative while the imaginary part becomes large).

We show in Fig. 4 the ηd elastic cross section predicted by the seven models. The figure illustrates that the cross section at threshold increases by one order of magnitude, from model 0 to model 6, i.e., from Re $a_{\eta N} = 0.42$ fm to Re $a_{\eta N} = 1.07$ fm: the strength of the ηd final-state interaction in the reaction $np \to \eta d$ depends naturally on the value of Re $a_{\eta N}$.

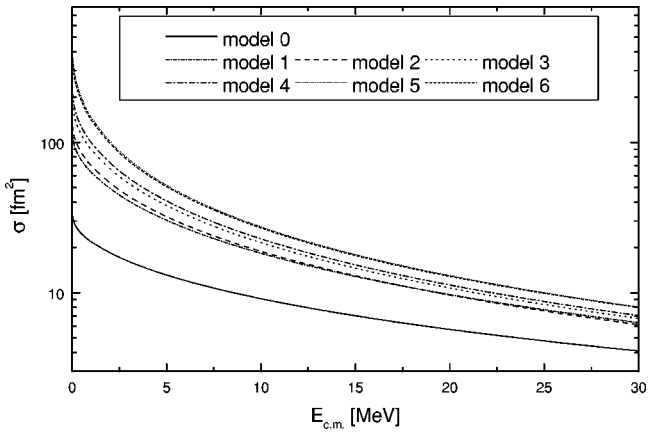

FIG. 4. ηd elastic scattering cross section obtained using the seven models of the coupled ηN-πN-σN system.

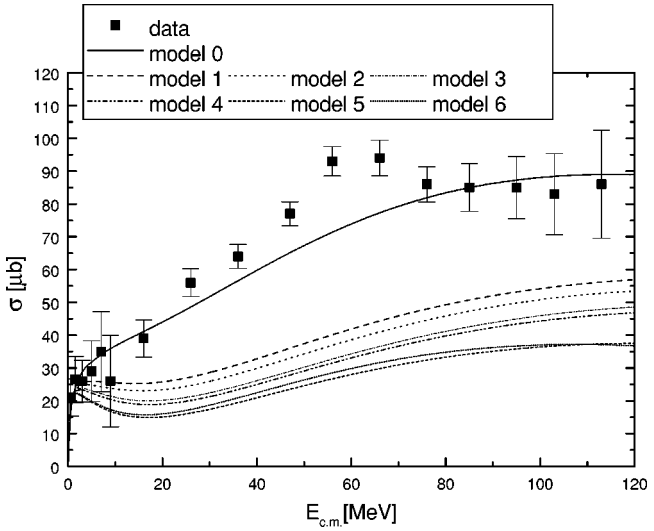

FIG. 5. Cross section of the reaction $np \to \eta d$ for the seven models described in the text as compared with the data of Refs. [1,2].

B. The reaction $np \to \eta d$

Our model of the $np \to \eta d$ reaction depicted in Fig. 3 has the ηNN coupling constant as an input. However this coupling is poorly known. The situation is no better for the coupling constants of the heavy mesons with the nucleon and with the S_{11} isobar. Therefore, at the first stage of our study we consider the model of Fig. 3 without heavy meson exchanges and use the data of $np \to \eta d$ to try to fix the ηNN coupling constant. In this attempt we noticed that the results differ considerably whether one uses the pseudovector vertex (35) or the pseudoscalar one (38). This vertex dependence comes exclusively from the direct production diagram of Fig. 3(a), since the box diagram gives almost exactly the same results with either type of coupling. We found that at this stage the pseudoscalar vertex (which leads to a negligible contribution for the direct term) allows us to obtain a better description of the experimental data. We show this result in Fig. 5, where after having fitted for each model the very-near-threshold region (see Fig. 6) we predicted from there

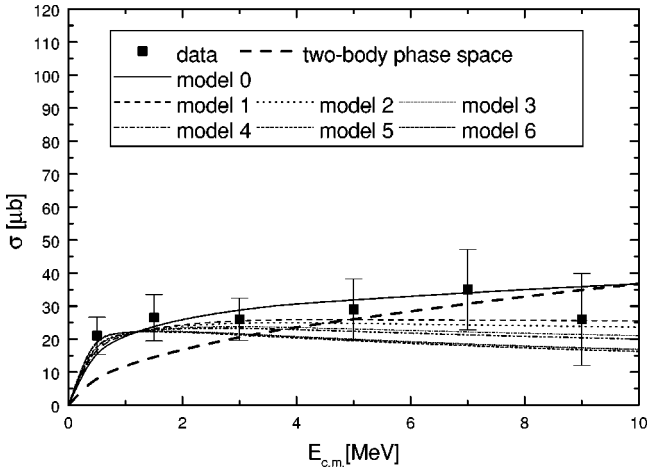

FIG. 6. Same as Fig. 5 but for the region very near threshold.

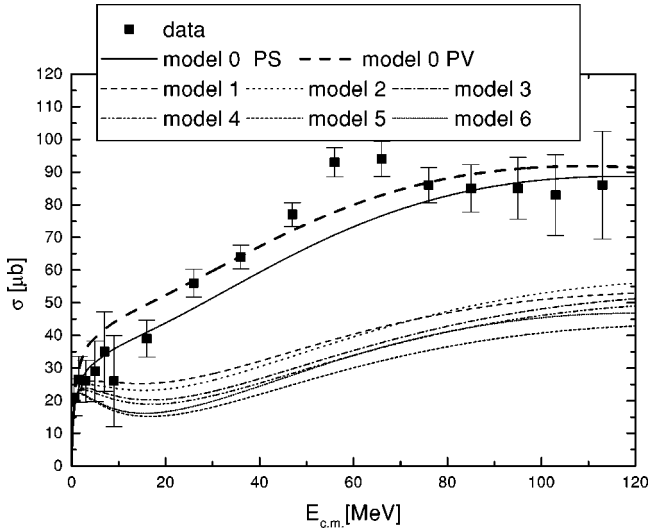

FIG. 7. Same as Fig. 5 but with the inclusion of the heavy pseudoscalar meson η'.

the cross section at higher energies.

It is clear from Figs. 5 and 6 that

(i) the very low-energy region (<10 MeV in the c.m.) is not the suitable kinematic domain for the $np \to \eta d$ reaction to probe the several ηN dynamical models, since the data does not distinguish and select between them;

(ii) however, the higher-energy region clearly favors model 0, the only one which describes the data reasonably well throughout the full energy range.

Besides, as we will see below, this preference of the data for a model with small Re $a_{\eta N}$ is to a large extent independent of the production mechanism, indicating that the characteristic shape of the experimental cross section is a signature of the ηd final-state interaction alone, whereas its absolute value involves the contribution of several different processes. This result is not so surprising since as we mentioned in the Introduction this system has a very strong ηd

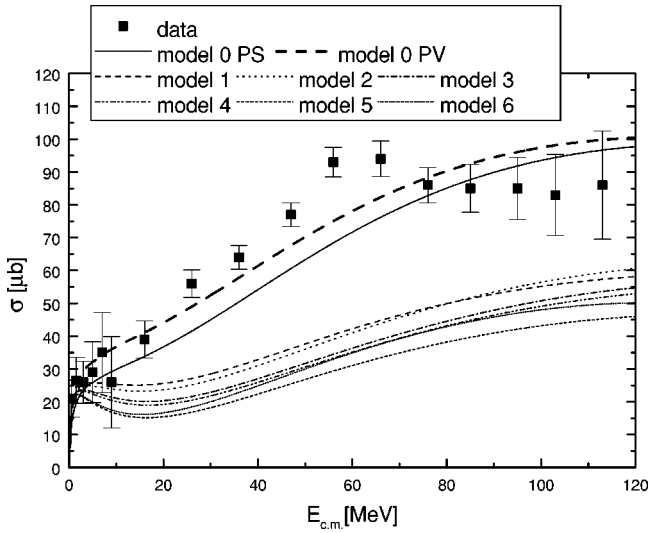

FIG. 8. Same as Fig. 5 but with the inclusion of the heavy scalar meson σ'.

interaction in the final state and therefore it follows from Watson's theorem [31] that the shape of the cross section will be determined basically by this final-state interaction.

The values of the ηNN coupling constant that we extract from this analysis are $f_\eta = 10.0$, 6.16, 8.03, 7.1, 6.77, 7.52, and 11.9, for models 0 to 6. These coupling constants are very large since if we consider $g_\eta = (2m_N/m_\eta) f_\eta$ we will get for model 0 $g_\eta^2/4\pi = 93.2$. This quantity is not well known but certainly it must be much smaller. For example, the Bonn potential [32] requires $2 < g_\eta^2/4\pi < 7$, while the Nijmegen potential [33] uses $g_\eta^2/4\pi = 0.25$, and the photoproduction process gives $1.0 < g_\eta 2/4\pi < 1.4$ [34] or even smaller values [35] from more recent data. Also, the light cone QCD sum rule [36] gives $g_\eta^2/4\pi = 0.3 \pm 0.15$. Thus, it seems that other processes have to contribute substantially to the production mechanism, in order to allow for a smaller ηNN coupling constant as dictated by several sources of evidence. The present lack of knowledge on these processes prevents the prediction of the ηNN coupling constant from the study of the $np \to \eta d$ reaction at this stage.

Accordingly, we include the exchange of a heavy meson (isoscalar, scalar, or vector) in the production mechanism, but used the fixed value $f_\eta = 1.5$, which corresponds to $g_\eta^2/4\pi = 2.1$, i.e., the lower limit determined from the Bonn potential. We show in Fig. 7 the results that are obtained by allowing in the production mechanism a pseudoscalar exchange corresponding to the η' meson. Once more, the shape of the cross section can only be reproduced at all energies by model 0, and the theoretical cross sections are actually very similar to those of Fig. 5. We adjusted the product of the coupling constants of the η' with the nucleon and with the S_{11} for models 0 to 6. Since the ηNN coupling constant is now much smaller, the relative importance of the direct term in the production amplitude is reduced and the difference between pseudovector and pseudoscalar coupling becomes less drastic. This is shown by the thick-dashed line in Fig. 7, which corresponds to model 0 and the coupling constant values of the solid line, but where the pseudovector vertex (35) is used instead.

We show in Fig. 8 the results obtained when instead of the η' the mechanism of meson production includes the exchange of a σ' [the $f_0(980)$]. The product of the coupling constants of the σ' with the nucleon and with the S_{11} were adjusted again for models 0 to 6. Once again, only model 0 gives more or less reasonable results and there is not much difference between the results of pseudovector and pseudoscalar coupling. In the case of vector-meson exchange, the dominant contribution, which corresponds to total orbital angular momentum $L = 0$, has exactly the same structure as the one of the pseudoscalar-meson exchanges considered and therefore the results would be similar to those of Fig. 7.

Finally, we conclude from the results of Figs. 7 and 8 that different short-range mechanisms can be adjusted to the magnitude of the cross section. Most importantly is that, nevertheless, the good description provided by model 0 for all energies, and essential for the ηd dynamics in the final state, is independent of the production mechanism considered.

C. Conclusions

We calculated the $np \to \eta d$ cross section by

(i) doing a three-body Faddeev calculation of the final-state interaction,

(ii) generating an initial-state wave function with a complex phenomenological two-nucleon potential, which reproduces well the $^1P_1$ phase shifts and the nucleonic inelasticities in the region near the η production threshold, and

(iii) testing several ηN interactions consistent with recent data analyses of the empiric $\eta N \to \eta N$ transition amplitudes, and also with the measured $\pi^- p \to \eta n$ total cross section.

We first verified that the determination of the ηNN coupling strength from this reaction depends crucially on the meson production mechanisms. Moreover, a reasonable value for that coupling demands the contribution of short-range processes; thus effort is still needed to further narrow the experimental uncertainty on the ηNN coupling constant from other processes, such that fixing the strength of these short-range mechanisms becomes possible.

The general concluding remarks from this work are

(i) the shape of the $np \to \eta d$ cross section within a wide energy range can only be explained by an ηN interaction model corresponding to a small scattering length (e.g the Jülich model); this is independent of the meson production mechanisms considered, and

(ii) in the region very close to threshold (< 10 MeV), the enhancement effect due to the final-state ηd interaction can be predicted by ηN interactions with very different strengths, provided that the production mechanisms are conveniently adjusted; it is the higher energy region which excludes the large scattering length ηN models. It follows that both domains of energy have to be taken into consideration in any data analysis, as done in Ref. [16,37], for instance.

ACKNOWLEDGMENTS

This work was supported in part by COFAA-IPN (México) and by Fundação para a Ciência e a Tecnologia, MCT, under Contract Nos. PRAXIS/P/FIS/10031/1998, SAPIENS/36291/99, and CERN/P/FIS/40135/2000 (Portugal).

[1] H. Calén *et al.*, Phys. Rev. Lett. **79**, 2642 (1997).
[2] H. Calén *et al.*, Phys. Rev. Lett. **80**, 2069 (1998).
[3] T. Ueda, Phys. Rev. Lett. **66**, 297 (1991).
[4] H. Garcilazo and M.T. Peña, Phys. Rev. C **61**, 064010 (2000).
[5] H. Garcilazo and M.T. Peña, Phys. Rev. C **63**, 021001(R) (2001).
[6] N.V. Shevchenko, S.A. Rakityansky, S.A. Sofianos, V.B. Belyaev, and W. Sandhas, Phys. Rev. C **58**, R3055 (1998).
[7] A. Deloff, Phys. Rev. C **61**, 024004 (2000).
[8] R.S. Bhalerao and L.C. Liu, Phys. Rev. Lett. **54**, 865 (1985).

[9] C. Bennhold and H. Tanabe, Nucl. Phys. **A350**, 625 (1991).
[10] N. Kaiser, T. Waas, and W. Weise, Nucl. Phys. **A612**, 297 (1997).
[11] M. Batinić, I. Šlaus, A. Švarc, and B.M.K. Nefkens, Phys. Rev. C **51**, 2310 (1995).
[12] M. Batinić, I. Dadić, I. Šlaus, A. Švarc, B.M.K. Nefkens, and T.-S.H. Lee, Phys. Scr. **58**, 15 (1998).
[13] A.M. Green and S. Wycech, Phys. Rev. C **55**, R2167 (1997).
[14] A.M. Green and S. Wycech, Phys. Rev. C **60**, 035208 (1999).
[15] C. Wilkin, Phys. Rev. C **47**, R938 (1993).
[16] A. Sibirtsev, S. Schneider, Ch. Elster, J. Haidenbauer, S. Krewald, and J. Speth, Phys. Rev. C **65**, 044007 (2002).
[17] C.D. Frogatt and J.L. Petersen, Nucl. Phys. **B129**, 89 (1977).
[18] H. Zankel, W. Plessas, and J. Haidenbauer, Phys. Rev. C **28**, 538 (1983).
[19] I.R. Afnan and A.W. Thomas, Phys. Rev. C **10**, 109 (1974).
[20] H. Garcilazo and T. Mizutani, *πNN Systems* (World Scientific, Singapore, 1990).
[21] F. Gross, J.W. Van Orden, and Karl Holinde, Phys. Rev. C **45**, 2094 (1992).
[22] R. Machleidt, K. Holinde, and C. Elster, Phys. Rep. **149**, 1 (1987).
[23] K. Holinde, Phys. Rep. **68**, 121 (1981).
[24] R.A. Arndt, C.H. Oh, I.I. Strakovsky, R.L. Workman, and F. Dohrmann, Phys. Rev. C **56**, 3005 (1997).
[25] M. Batinć, A. Švarc, and T.-S.H. Lee, Phys. Scr. **56**, 321 (1997).
[26] V.Yu. Grishina, L.A. Kondratyuk, M. Buscher, J. Haidenbauer, C. Hanhart, and J. Speth, Phys. Lett. B **475**, 9 (2000).
[27] C. Hanhart and K. Nakayama, Phys. Lett. B **454**, 176 (1999).
[28] Göran Fäldt and Colin Wilkin, Phys. Scr. **64**, 427 (2001).
[29] A. Fix and H. Arenhövel, Eur. Phys. J. C **9**, 119 (2000); nucl-th/0006074.
[30] S. Wycech and A.M. Green, nucl-th/0104053.
[31] Kenneth M. Watson, Phys. Rev. **88**, 1163 (1952).
[32] R. Machleidt, Adv. Nucl. Phys. **19**, 189 (1989).
[33] T. Rijken and V.G.J. Stoks, Phys. Rev. C **59**, 21 (1999).
[34] M. Benmerrouche and N.C. Mukhopadhyay, Phys. Rev. Lett. **67**, 1070 (1991).
[35] L. Tiator, C. Bennhold, and S.S. Kamalov, Nucl. Phys. **A580**, 455 (1994).
[36] Shu-Lin Zhu, Phys. Rev. C **61**, 065205 (2000).
[37] S. Wycech and A. M Green, Phys. Rev. C **64**, 045206 (2001).